Adaptive Virtual Resistance Load Sharing for Resistive Microgrids

Augustine M. Egwebe, Meghdad Fazeli, Paul Holland

Electrical and Electronic Engineering Department, Swansea University, UK

Abstract

This paper proposes an adaptive virtual resistance load sharing method in $\alpha\beta$ frame, where the α-component of the virtual resistance is used to share the active power and the β-component of the virtual resistance is used to share reactive power. Using the proposed method for photovoltaic systems makes the active and reactive power sharing sensitive to the varying nature of the solar energy. It will be shown that the proposed adaptive active power sharing significantly reduces the energy required from a fossil-fuelled auxiliary generator. The proposed adaptive reactive power sharing reduces the reactive power exchanged with the auxiliary generator and the switching stress on each distributed generator's converter through, seamlessly, reducing the reactive power contribution of the units with higher active power contribution. This is all achieved without any communication between distributed generation units. Whilst the proposed method is also applicable on inductive microgrids, this paper focuses on a resistive microgrid since most microgrids are likely to be located on the low voltage side of the grid (where the network is mainly resistive). Different load sharing methods in a resistive microgrid are also categorized and briefly reviewed to justify the chosen approach in the paper. MATLAB/SIMULINK simulations are used to validate the proposed method.

Keywords: Distributed Generation, Microgrids, Virtual Resistance, Photovoltaic, Renewable Energy Sources

*Corresponding author
Email address: augustine.egwebe@swansea.ac.uk (Augustine M. Egwebe)

1. Introduction

Sustainable energy generation, and efficient energy storage and management are possible in well-controlled microgrids (MGs) enabling a global move from large centrally controlled power stations to a distributed generation approach where smaller renewable based generators can be successfully employed [1–4]. Thus MGs, consisting of a variety of distributed units, enable capacity and control flexibilities that provide energy security, system reliability and power quality gains [5–7]. The MG can be controlled to operate both in grid-connected approach or in islanded mode. Renewable energy generation is often complemented with dispatchable resources, such as auxiliary generator (AG) and energy storage systems, to balance demanded energy with generation in an MG [6]; the absence of such dispatchable resources can cause the malfunctioning of the inverter-based units [8–11]. Hybrid distributed generation networks comprising of renewable sources, energy storage systems and fossil-fuelled AG, are often employed to improve the flexibility and reliability of MGs [1–3, 12]. In grid-connected MGs, local voltage and frequency are imposed by the grid; whereas, in islanded-mode, the inverter-based source must actively regulate the voltage and frequency for the stable and continuous operation of the MG [13–15]. In case of shortage of energy when islanded, a practical MG needs a fossil-fuelled AG to supply (at least) the essential loads. The operation of the AG, in this approach (which operates only as a back-up), is different to that of a master unit (in a master-slave paradigm) since the operations of other units are not reliant on the AG.

Most MGs are likely to be located at low voltage side of the grid, where the network is predominately resistive [16–18]. In resistive MGs, three main load sharing methods were identified in the literature:

1.1. P-V and Q-f Droop Load Sharing Scheme

In predominantly resistive systems, the droop slopes are defined as active power (P)-voltage (V) and reactive power (Q)-frequency (f). Similar to classical inductive networks, P and Q are used to regulate the voltage amplitude and frequency of the distributed generator (DG)[9, 13, 19, 20]. In a resistive MG, P and Q are given by

[20–22]:

$$P = \frac{V_o^2 - V_o V_t \cos\delta}{Z} \approx \frac{V_o}{R}\Big(V_o - V_t\Big)$$
$$Q = \frac{V_o V_t}{Z}\sin\delta \approx -\frac{V_o V_t}{R}\delta \tag{1}$$

The droop equation (given in (1) and (2)) is normally adopted for the proportional sharing of P and Q; where P and Q vary according to the DG's voltage and frequency respectively [20–22]:

$$V_o = V^* - m_p\big(P - P^*\big); \quad m_p = \frac{\Delta V}{P_{rated}}$$
$$\omega = \omega^* + n_q\big(Q - Q^*\big); \quad n_q = \frac{\Delta\omega}{Q_{rated}} \tag{2}$$

where $(V_o - V_t)$ is the difference in voltage amplitude; δ is the difference in phase angle between the DG's output voltage (V_o) and the voltage at the point of common connection (V_t); R is the resistance of the output feeder of the DG in the resistive network. ΔV and $\Delta\omega$ define the allowed voltage and frequency deviation. m_p and n_q define the droop coefficients (i.e., the gradient of droop lines in Fig. 1), which guarantee the preferred relative power sharing based on the rating of the inverter-based source (i.e., P_{rated} and Q_{rated}).

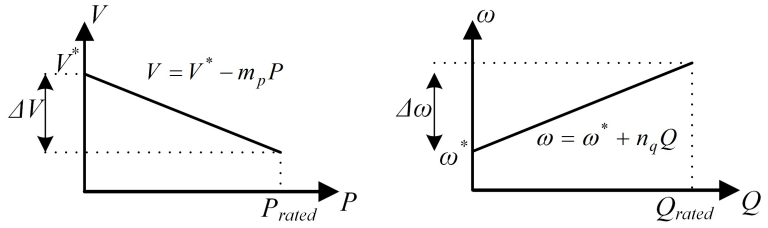

Figure 1: Active and reactive power droop characteristic (in steady-state) in a resistive MG

The droop slopes (in Fig. 1) are carefully selected to promote and ensure adequate load sharing between DGs while minimizing significant deviation in frequency and voltage at steady state [20].

1.2. P-f and Q-V Droop with Virtual Impedance

References [16, 19, 23, 24] have investigated the "Virtual Impedance" (VI) scheme to mitigate the coupling effect amongst P and Q, which is due to the relatively higher

line resistance in a low voltage network.

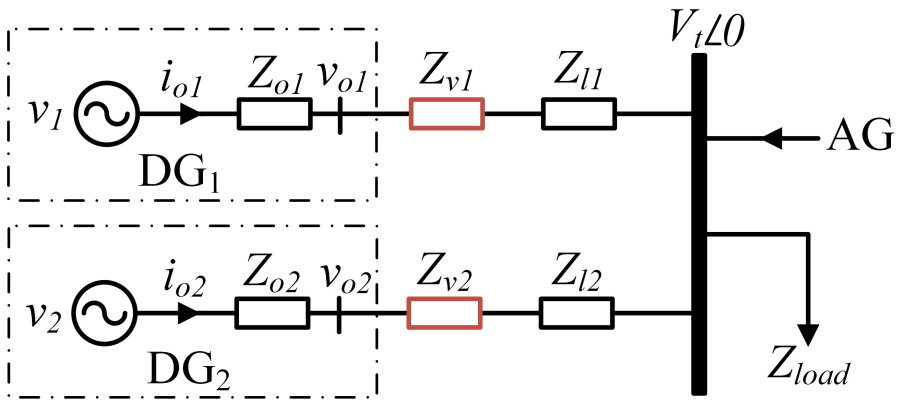

Figure 2: Two parallel-connected DGs including virtual impedance

Figure 2 shows an equivalent circuit of two parallel-connected DGs with VIs, where v_{o1}, i_{o1}, Z_{o1} , Z_{v1} , and Z_{l1} are the output voltage, output current, output impedance, virtual impedance and line impedance of DG_1. v_{o2}, i_{o2}, Z_{o2} , Z_{v2} , and Z_{l2} are the output voltage, output current, output impedance, virtual impedance and line impedance of DG_2; V_t is the terminal bus voltage of the MG. The VI is usually wired in series with the resistive line impedance to make the overall output impedance of the DG inductive, this, in turn, improves the stability and transient performance of the system [25, 26]. Since using the VI, the effective total impedance becomes inductive, the classical *P-f* and *Q-V* droops can be employed [22].

1.3. Virtual Impedance Load Sharing Scheme

The VI scheme is often used in inverter-based applications to shape the dynamic profile of DG. Power flow control and harmonic compensation can also be achieved via the VI scheme [19, 24]. The VI scheme also has the potential to autonomously enhance current sharing between parallel-connected converters in an MG, this in turn eliminates the need for the classic droop controller [17, 18, 27]. It was shown in [17] and [18] that the VI, coupled with a synchronous reference frame phase-locked loop (PLL), could be used as an alternative option for load current sharing in parallel-connected

DGs in an MG. Hence, the VI scheme help to eliminates some of the major drawbacks of conventional droop control schemes, i.e., inaccurate load sharing, instability problems as a result of load disturbance, poor transient response, steady-state error in line voltage, and frequency [16–18, 27–29].

Out of the three above described approaches, the *P-V*, *Q-f* droops approach is the simplest. However, it has the disadvantage of relatively unstable operation in comparison with VI that improves the system stability [17–20, 27, 30, 31]. Having both droops (*P-f* and *Q-V*) and VI, although possible, seems redundant as only VI can be used for load sharing. Therefore, the rest of the paper mainly concentrates on the VI load sharing approach.

In a microgrid consisting of several PV units, the solar irradiation on the units will not be necessarily the same even if they are located in a small geographical area. This can be due to the shadow of passing clouds or a nearby object such as trees. A common drawback of all of the previous arts in load sharing in resistive MGs (using any of the above approaches) is that the sharing ratio (between units) is not sensitive to the varying nature of renewable energy. Figure 3 shows a conventional VI (*I-V*) load sharing scheme where a static voltage droop gain is determined regardless of the energy available from the renewable energy source. The DG's local voltage in this manner varies in relation to changes in either the load or line impedance, the voltage is usually constrained within the acceptable voltage drop, to maintain the DG's local voltage within acceptable limits [20]. In such cases, if the available power in a DG reduces from I_1 to $I_1^{'}$ (e.g., say there is a drop in solar irradiation), the local voltage (V) of the DG will shift to a new operating point (V^*). Subsequently, the other connected DG must comply with the new operating voltage (V^*), leading to its power drop from I_2 to $I_2^{'}$ (irrespective of its available generating capacity), which can increase the energy demanded from an AG.

Similarly, Q sharing, conventionally, is only sensitive to the inverter's rating (S_{rated}) of each DG. I.e., a unit with higher P contribution would also contribute more Q. This is obviously not an optimised sharing as it can increase the switching stress on the inverters as well as the Q exchanged by the AG.

Unlike [32], where only dynamic *P-f* droop in an inductive MG is considered,

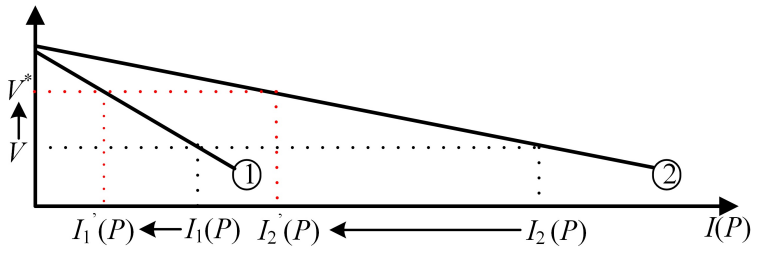

Figure 3: Characteristics of static virtual resistance droop (V-P)

the current paper uses an adaptive virtual resistance scheme (in $\alpha\beta$ frame) to optimise both P and Q sharing. In addition to the comprehensive P and Q sharing, the proposed method in this paper is based on the VI which curbs the inherent stability problem associated with the droop control [17–20, 27, 30, 31]. The proposed method avoids overloading of each DG through sharing the load according to the available generation capacity of each unit, where P is shared using the α-component of the virtual resistance and Q is shared using the β-component of the virtual resistance. The proposed adaptive approach additionally considers the rating, output impedance, and voltage and frequency limits of each unit. To achieve this, the photovoltaic (PV) array's current vs. voltage characteristics is used in defining an operating range according to the DC link voltage variations due to fluctuations in solar irradiation. An adaptive Q sharing is also presented which reduces the inverters' switching stress through, seamlessly, reducing the Q contribution of units with higher P contribution while the inverters' ratings are maintained. This will also minimize Q exchanged with an AG since the DGs can dynamically compensate for one another. The control of an AG to provide P and Q compensation in a low voltage MG is also presented.

2. Microgrid Network Under Study

Figure 4 illustrates an islanded MG with two three-phase PV systems (DG_1, DG_2) in a resistive (low voltage) network. The flow of energy from a nearby fossil-fuelled AG, using local information from the DGs, is regulated using the power electronic converter (PEC). The three-phase inverter-based sources are PWM controlled with the classical cascaded voltage and current control loops [16–18, 27, 31].

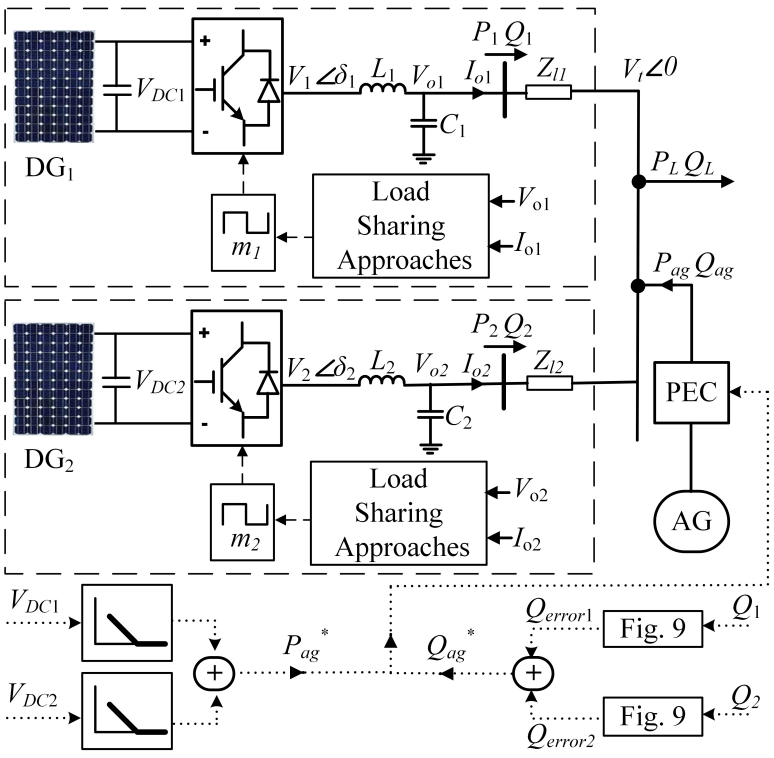

Figure 4: Microgrid network under study with resistive line impedances

3. Proposed Adaptive Virtual Resistance Sharing

3.1. Virtual Resistance Load Sharing

By using KVL, an expression for the output voltage of a DG unit (see Fig. 2) in relation to the VI is given in $\alpha\beta$ frame as follows:

$$\begin{aligned} v_{o\alpha} &= v^*_{\alpha} - \left(R_{v\alpha} i_{o\alpha} - X_v i_{o\beta}\right) \\ v_{o\beta} &= v^*_{\beta} - \left(R_{v\beta} i_{o\beta} + X_v i_{o\alpha}\right) \end{aligned} \tag{3}$$

where R_v and X_v are virtual resistance and virtual inductance, respectively. The X_v component of Z_v makes the DG's output impedance more inductive in order to vastly improve the decoupling between *P* and *Q*. Besides enhancing current sharing capability, the R_v component of Z_v also restricts the voltage drop within a small range. R_v is often selected to drop the output voltage up to 2 - 5% of the nominal

voltage, to meet the acceptable voltage regulation and promotes the characteristics of current sharing.

Since the line is predominately resistive in a low voltage MG (and X_v is exploited to improve the decoupling between *P* and *Q*), R_v is used for *P* and *Q* sharing. Hence, this paper proposes the use of the α-component of the virtual resistance $R_{v\alpha}$ to regulate active power (*P*-*V*) sharing; while the β-component of the virtual resistance $R_{v\beta}$ is chosen for reactive power (*Q*-*f*) sharing, respectively, which is demonstrated below:

The virtual resistance makes the voltage drops as current increases. Therefore, it can be used to define the sharing ratio of the units. The voltage drop by the virtual resistance in $\alpha\beta$ frame is:

$$\begin{aligned} v_{o\alpha} &= v_{\alpha}^{*} - R_{v\alpha} i_{o\alpha} \rightarrow \Delta v_{o\alpha} = R_{v\alpha} i_{o\alpha} \\ v_{o\beta} &= v_{\beta}^{*} - R_{v\beta} i_{o\beta} \rightarrow \Delta v_{o\beta} = R_{v\beta} i_{o\beta} \end{aligned} \tag{4}$$

Using the Inverse Park Transform and the fact that PLL makes $V_q = 0$ at steady state, one can write:

$$\begin{aligned} v_{o\alpha} = V_{od}\cos\delta - V_{oq}\sin\delta \quad &\xrightarrow{\text{PLL } (V_q=0)} \quad v_{o\alpha} = V_{od}\cos\delta \\ v_{o\beta} = V_{od}\sin\delta + V_{oq}\cos\delta \quad &\xrightarrow{\text{PLL } (V_q=0)} \quad v_{o\beta} = V_{od}\sin\delta \end{aligned} \tag{5}$$

Since using X_v, the total output impedance is mainly inductive, δ is relatively small. Thus, at steady state, $(\cos\delta) \rightarrow 1$ and $(\sin\delta) \rightarrow \delta \approx 0$, which simplifies (5) as:

$$\begin{aligned} v_{o\alpha} = V_{od}\cos\delta \quad &\xrightarrow{\delta\rightarrow 0} \quad |v_{o\alpha}| \rightarrow V_{od} \\ v_{o\beta} = V_{od}\sin\delta \quad &\xrightarrow{\delta\rightarrow 0} \quad |v_{o\beta}| \rightarrow V_{od}\delta \end{aligned} \tag{6}$$

Therefore, the active and reactive powers in $\alpha\beta$ frame are:

$$\begin{aligned} P = 1.5\Big(v_{o\alpha}i_{o\alpha} + v_{o\beta}i_{o\beta}\Big) \quad &\xrightarrow{|v_{o\beta}|\rightarrow 0 \text{ and } |v_{o\alpha}|\rightarrow V_{od}} \quad P = 1.5\Big(V_{od}i_{o\alpha}\Big) \\ Q = 1.5\Big(v_{o\beta}i_{o\alpha} - v_{o\alpha}i_{o\beta}\Big) \quad &\xrightarrow{|v_{o\beta}|\rightarrow 0 \text{ and } |v_{o\alpha}|\rightarrow V_{od}} \quad Q = -1.5\Big(V_{od}i_{o\beta}\Big) \end{aligned} \tag{7}$$

Equation (7) shows that the *P* can be controlled by $i_{o\alpha}$, and the *Q* can be controlled by $i_{o\beta}$. Moreover, substituting (6) into (4) gives:

$$\begin{aligned} \Delta V_{od} &= R_{v\alpha} i_{o\alpha} \\ V_{od}\Delta\delta &= R_{v\beta} i_{o\beta} \end{aligned} \tag{8}$$

Calculating $i_{o\alpha}$ and $i_{o\beta}$ from (7), and substituting them into (8) gives:

$$\begin{aligned}(1.5V_{od})\Delta V_{od} &= R_{v\alpha}P \\ (1.5V_{od}^2)\Delta\delta &= -R_{v\beta}Q\end{aligned} \tag{9}$$

Equation (9), by taking into account that $\omega = \int \delta \mathrm{dt}$, and $V_{od} \approx V^* = 1$ pu (at steady state), relates (2) (i.e., *P*-*V* and *Q*-f droop) to $R_{v\alpha}$ and $R_{v\beta}$:

$$\begin{aligned}V_o &= V^* - m_p\big(P - P^*\big); \quad m_p = \frac{\Delta V}{P_{rated}} = \frac{R_{v\alpha}}{1.5V^*} \\ \omega &= \omega^* + n_q\big(Q - Q^*\big); \quad n_q = \frac{\Delta\omega}{Q_{rated}} = \frac{R_{v\beta}}{1.5(V^*)^2}\end{aligned} \tag{10}$$

where ΔV and $\Delta\omega$ are the allowed voltage and frequency deviations. Using (10), $R_{v\alpha}$ and $R_{v\beta}$ can be determined to obtain the sharing characteristics of a classical droop using a virtual resistance in $\alpha\beta$ frame. Subsequently, the output power interaction between N parallel-connected DGs using (10) is expressed in (11):

$$\begin{aligned}P_1R_{v\alpha1} = P_2R_{v\alpha2} \quad &= \ldots = P_NR_{v\alpha N} \quad = \Delta V \\ Q_1R_{v\beta1} = Q_2R_{v\beta2} \quad &= \ldots = Q_NR_{v\beta N} \quad = \Delta\omega\end{aligned} \tag{11}$$

Equations (10) and (11) show that *P* and *Q* can be independently controlled using $R_{v\alpha}$ and $R_{v\beta}$ respectively. Using virtual resistance in $\alpha\beta$ frame (i.e. (10)) to achieve independent *P* and *Q* sharing provide a much simpler design procedure, compared to previous arts [16–18, 25]. However, similar to previous works, the proposed virtual resistance sharing scheme still suffers from insensitivity to the input power variation of the DG due to variation in the renewable energy source (e.g., solar irradiation). According to Fig. 3, if the available energy of one DG is not adequate to supply the static sharing ratios enforced by (11), a new operating voltage will be imposed on all other DGs connected to the network. Hence, other DGs are forced to operate at the new operating point irrespective of the generating capacity of the other DGs. I.e. a reduction in the generating capacity of one unit causes a drop in the generating capacity of all the other units' (see simulation results in Fig. 10 (b)), which may lead to a supply shortage. This energy shortage can be counterbalanced by the energy stored in the DC-links' capacitors which reduces the DC link voltage. Therefore, the DC link voltage can be utilized to activate an AG using a PEC to offset the energy shortage.

Obviously, the energy required from the AG is not minimised since the generation reduction is imposed on all units. This is because of the insensitivity of the fixed VI control scheme to the perturbing nature of the input renewable energy source (see Fig. 10).

3.2. Proposed Adaptive Load Sharing

A method to make active and reactive power sharing sensitive to solar irradiation (without the need for measuring it) is proposed in this section, such that when solar irradiation of one unit drops:

1. The other units do not drop their generation.
2. The other units increase their generation, provided that enough irradiation is available.
3. The units that generate less *P* contribute more in *Q*, and vice versa.

Reference [33] described the mathematical model of a PV array with *P-V* characteristic illustrated in Fig. 5. An average model for sinusoidal PWM three-phase inverters in $\alpha\beta$ frame is explained in [8, 34]:

$$|V_{\alpha\beta}| \approx \frac{1}{2} |m_{\alpha\beta}| V_{DC} \tag{12}$$

where $V_{\alpha\beta}$ is the $\alpha\beta$ frame component of the inverter' fundamental AC voltage, $m_{\alpha\beta}$ is the modulating index (in the $\alpha\beta$ frame), and V_{DC} is the DC link voltage. In PV systems, the V_{DC} continually changes as the solar irradiance level *G* and/or demanded load P_{Load} varies. Thus, as V_{DC} drops (e.g. due to a *G* reduction), $|m_{\alpha\beta}|$ needs to increase in order to maintain $|V_{\alpha\beta}|$ according to (12). For $|m_{\alpha\beta}| = 1$, $|V_{\alpha\beta}|$ will depend only on V_{DC} (as $|m_{\alpha\beta}| \leq 1$). Therefore, an additional decrease in V_{DC} will decrease $|V_{\alpha\beta}|$. Subsequently, the selected minimum DC voltage V_{DC-min} must ensure (12) while $|m_{\alpha\beta}| = 1$, to precisely regulate the AC output voltage of the DG. For example, for an RMS 230 V DG system, $V_{DC} \geq 650.54$V (i.e. the operating point limit in the case where the modulating index, $|m_{\alpha\beta}| = 1$). Thus, the PV array must be appropriately designed such that the DC voltage of the maximum power at a small irradiation (say 0.05 pu) = $V_{DC-min} \approx 650.54$V (see Fig. 5).

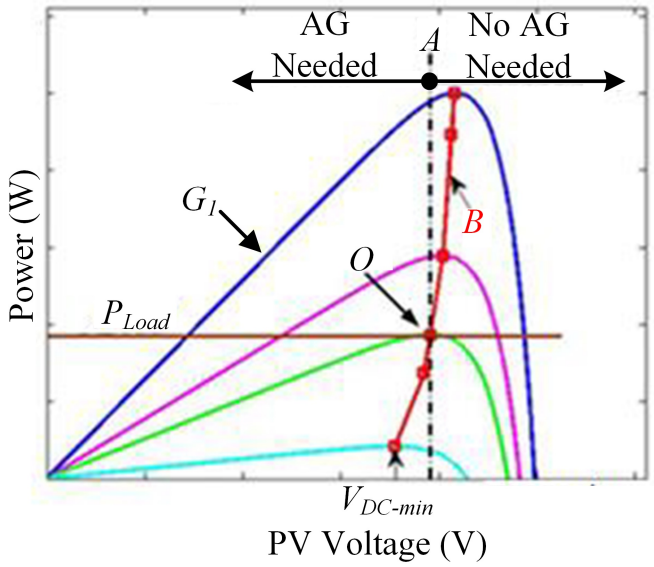

Figure 5: PV power vs.voltage curve for various solar irradiance level. (Curve B): Maximum point curve; (P_{Load}): Constant load demand curve

The AC side load determines the operating point of the PV in the absence of maximum power tracking in islanded mode. Furthermore, as shown in Fig. 5, as the irradiance level and/or load varies, the V_{DC} will continuously vary from the minimum operating voltage (V_{DC-min}) to the PV array's open circuit voltage (V_{OC}). The adaptive load sharing scheme proposed in this paper uses the variation in V_{DC} in conditioning the classical static load sharing schemes for an optimized load sharing. This is done via the linear approximation of the PV maximum power point characteristic (curve B) and the subsequent adaptation of the virtual resistance according to the linearized curve. When the available solar power of the DG is greater than the load, the DG operates typically within its operating zone (right-hand side of curve B in Fig. 5). As G reduces, the DG keeps supplying the load until the point when the available solar power is not adequate to supply the load (point O); the AG is subsequently activated (when V_{DC} become less than a threshold) to offset the energy shortage. It is noted that in the presence of an energy storage unit, the energy level of the storage unit can be used as an indicator for the lack of energy rather than the DC-link voltage.

In order to make sure that when the input solar power of one unit drops; the other units do not follow it, the sharing scheme must be sensitive to the available input power. However, since measuring solar irradiance is not practical, this paper proposes to make the load sharing scheme varies according to the maximum power curve (i.e., curve B in Fig. 5), which is linearized and shown in (13) [35]:

$$P_{DC-max} = k_n V_{DC-opt-n} + c_n \tag{13}$$

where k_n and c_n are gains to get a linear approximation of the maximum power curve of the nth PV array. $V_{DC-opt-n}$ is the DC link voltage of the nth PV array when the PV power is maximum (i.e., curve B in Fig. 5).

As the PV power P_{pv} varies, the available reactive power capacity (Q_{avail}), which can be exchanged by the inverter, varies according to (14) [8]:

$$Q_{avail} = \sqrt{(S_{rated})^2 - (P_{pv})^2} \tag{14}$$

In (14), Q_{avail} increases for a reduction in G of a DG unit. Thus, an optimized sharing scheme must have the following characteristics:

1. All units must generate active power according to curve B (Fig. 5)
2. Units with higher P contributions must have a lower Q contribution since Q_{avail} reduces as P_{pv} increases.

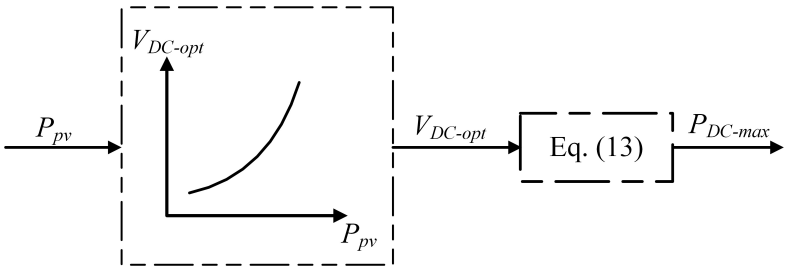

Figure 6: A proposed method to impose curve B (see Fig. 5) on virtual resistance control scheme.

In order to make sure that the PV systems operate on curve B as load varies, Fig. 6 is proposed. In Fig. 6, the measured PV power P_{pv} is passed through V_{DC-opt} vs. P_{pv} curve, explained in [35], to get V_{DC-opt} which is used in (13) to get P_{DC-max}. Using Fig. 6 will create a closed loop which makes $P_{pv} = P_{DC-max}$ at steady state.

P_{DC-max} will be used for sharing active power, and Q_{avail} will be used for sharing reactive power (explained below). At steady state $P_{pv} = P_{DC-max}$,which means that the maximum power from each unit will be generated if it is required by the load while taking into account the rating (S_{rated}), output impedance and voltage limits of each unit.

3.3. Adaptive Virtual Resistance Load Sharing Scheme

This section explains the adaptive virtual resistance control scheme where the coefficients of the virtual resistance are adjusted as V_{DC} changes (due to *G* variations). The proposed adaptive virtual resistance sharing scheme (in the $\alpha\beta$ frame) can be considered as tuning parameters to adjust the direct and quadrature components of the output currents of the parallel-connected DG units.

Combining the proposed adaptive *P* and *Q* sharing with the proposed virtual resistance droop discussed in (10), yields:

$$\begin{aligned} m_p &= \frac{\Delta V}{P_{DC-max}} = \frac{R_{v\alpha}}{1.5V^*} \rightarrow R_{v\alpha} = \frac{1.5V^*\Delta V}{P_{DC-max}} \\ n_q &= \frac{\Delta \omega}{Q_{avail}} = \frac{R_{v\beta}}{1.5(V^*)^2} \rightarrow R_{v\alpha} = \frac{1.5(V^*)^2\Delta \omega}{Q_{avail}} \end{aligned} \tag{15}$$

The adaptive load sharing ratios, for an MG consisting of two DGs, can thus be explained in (16). Using (15), $R_{v\alpha}$ is sensitive to solar irradiation through P_{DC-max}, and $R_{v\beta}$ is sensitive to P_{pv} through Q_{avail}.

$$\frac{P_1}{P_2} = \frac{R_{v\alpha 2}}{R_{v\alpha 1}} = \frac{P_{DC-max-1}}{P_{DC-max-2}} \text{ and } \frac{Q_1}{Q_2} = \frac{R_{v\beta 2}}{R_{v\beta 1}} = \frac{Q_{avail-1}}{Q_{avail-2}} \tag{16}$$

Moreover, since *P* and *Q* are perfectly decoupled using X_v, a decrease in the solar irradiation of one unit increases $R_{v\alpha}$, which in turn reduces *P* (according to (15)). The reduction in $P_{pv} = P_{DC-max}$ causes an increase in Q_{avail}, which reduces $R_{v\beta}$, which in turn increases *Q* (according to (15)). Since other units are also controlled using the proposed adaptive virtual resistance (i.e. (16)), they will adjust their *P* and *Q* accordingly to supply the load and to comply with the voltage and frequency standards. Also, Q_{avail} of a DG unit increases with decreasing irradiation according to (14). In the case of static virtual resistance scheme, a fixed *Q*-droop gain is set irrespective of

Q_{avail}, hence Q sharing is not optimized, which leads to excessive switching stress and subsequent possible inverter over-loading. However, using the proposed scheme, as shown in Fig. 7, reduction in P_1 to $P_1^{'}$, causes P_2 to increase (assuming enough G). Hence, Q_{avail1} increases and Q_{avail2} reduces which according to (16) increases Q_1 and reduces Q_2 (see results in Fig. 12.e).

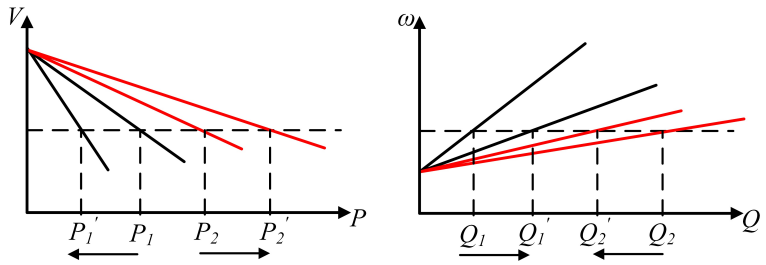

Figure 7: Illustration of the performance of the proposed adaptive virtual resistance for active and reactive power sharing

Fig. 8a illustrates the proposed adaptive virtual resistance sharing scheme in a resistive MG. The DG's control paradigm, shown in Fig. 8a, consists of an inner current loop, an outer voltage loop, and the proposed virtual resistance control scheme (i.e., Eq. (4) in Fig. 8a). Conventional cascaded voltage and current loops, using Proportional-Resonant (PR) controllers, are used to control the inverter. Stationary reference frame parameters are generated using Clarke transforms as implemented in [18]. As shown in Fig. 8a, a PLL is used to impose internal frequency synchronisation and set the reference frequency [36, 37]. Unlike in P-f droop, where system dynamics mainly depend on the low-pass filter of the power controller, the dynamics of the proposed control scheme is mainly dependent on the VI and the line impedances.

4. Auxiliary Generator Control

All practical islanded networks need an AG to supply at least the critical loads whenever there is a shortage of renewable energy. It is, of course, possible to consider demand-side management schemes prior to turning the AG ON (which is out of the scope of this paper).

(a)

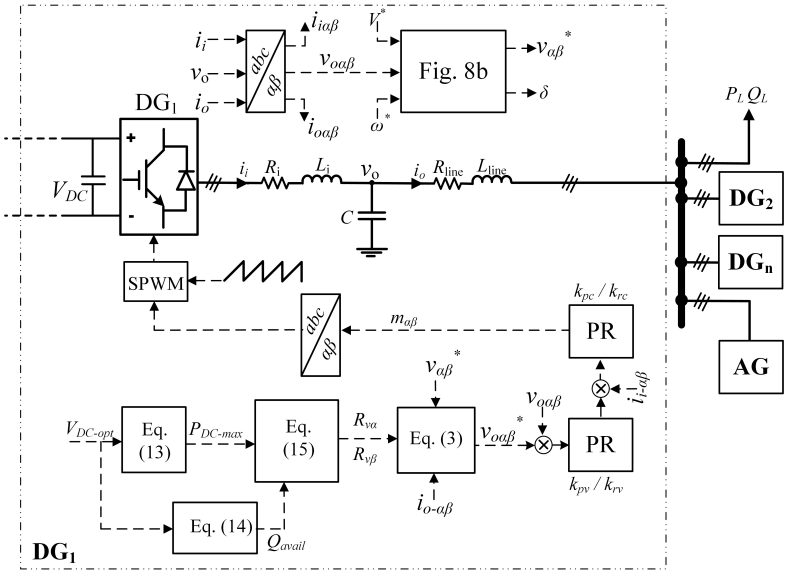

(b)

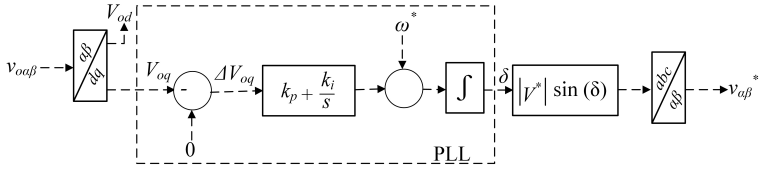

Figure 8: (a) Proposed adaptive virtual resistance load sharing scheme in a resistive MG; (b) Phase locked loop

4.1. Active Power Control

Active power compensation from the AG is regulated by using the V_{DC} of the DG as an indicator for energy shortage (see Fig. 4). Hence, following a decrease in the V_{DC} of either DGs below a threshold (here the threshold is 0.85pu), the AG is turned ON.

$$P_{ag}^{*} = K_{pag} \sum_{n=1}^{N} V_{DC-n} \tag{17}$$

4.2. Reactive Power Control

The idea is to exploit the inverters' capacity to supply reactive power without violating S_{rated}. Therefore, reactive power of each unit $Q \geq Q_{avail}$. To achieve this, as shown in Fig. 9, Q_{error} is generated by comparing the limited and the measured Q. Since Q_{avail} varies as P_{pv} varies, a variable hard-limit is needed. Theoretically, the hard-limit can be up to Q_{avail}; however, some safety margin (about 3%) is recommended to make sure that S_{rated} will not be violated due to the dynamics of the AG. Q_{error} of each unit will be added together to form the reference reactive power for the AG:

$$Q_{ag}^{*} = K_{qag} \sum_{n=1}^{N} Q_{error-n} \tag{18}$$

where K_{pag} and K_{qag} are the AG's proportional controller gains, the design of which is beyond the scope of this paper (a value between 1 to 10 is recommended depending on the dynamics of the AG).

Using the proposed method the available capacity of the PV inverter will be used to support the local voltage in triggering the AG using (17) and (18) and providing P and Q compensation without violating either the S_{rated} of the inverter or its voltage limitations. The references P_{ag}^{*} and Q_{ag}^{*} are fed into classical P-Q control loops to control the AG injected P and Q into the MG.

5. Simulation Results

The model shown in Fig. 4, with parameters explained in Table 1, was simulated using MATLAB-SIMULINK. The MG comprises of two PV systems and one AG feeding

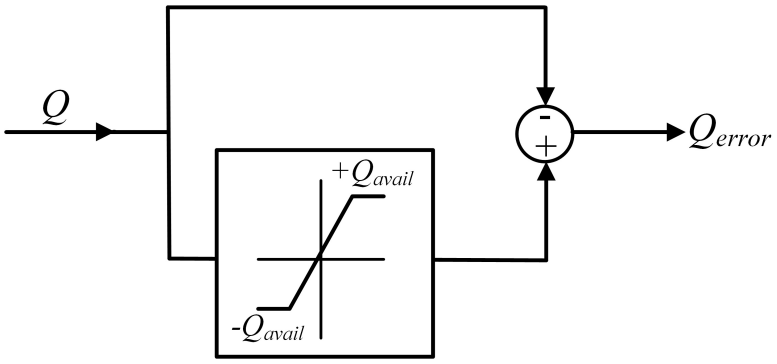

Figure 9: Reactive power compensation from each DG

a three-phase load (demanding both active and reactive power). Each PV systems have its control scheme (including virtual resistance loop), and the load sharing scheme is simulated for both static and adaptive virtual impedance methods. The inverters' ratings are: $S_{rated1} = S_{rated2} = 1.05\text{pu}_{pv}$ (pu_{pv} denotes pu based on the rating of the associated PV array). The simulation is tested for fixed active power load demand (P_{Load}) and reactive load demand (Q_{Load}) in the presence of variable solar irradiation.

Table 1: System's Parameter

Variable	**Value**	**Variable**	**Value**
V_{L-L}	415V	f^*	50Hz
S_{rated1} / S_{rated2}	0.6 / 0.4 (pu)	S_{Load}	0.875 (pu)
P_{Load} / Q_{Load}	0.75 / 0.45 (pu)	R_{line} / X_{line}	7.7
LC Filter	4mH / 16μF	k_{pv} / k_{rv}	0.09 / 86
k_1 and c_1(Eq.13)	76.48 and -50692.01	k_{pc} / k_{rc}	0.05 / 0
k_2 and c_2(Eq.13)	43.05 and -28442.60	k_p / k_i	1.2 / 1200
Length of line	0.5 km	C_{dc}	1200μF

5.1. Load Sharing in a Resistive MG using Virtual Resistance Scheme

This section compares the conventional static virtual resistance sharing with the proposed adaptive virtual resistance sharing, for the system shown in Fig. 4. Three

different load sharing scenarios were considered: static *P* and static *Q*, adaptive *P* and static *Q*, and finally adaptive *P* and adaptive *Q*. The simulation events are identical for all scenarios where P_{Load} = 0.75 pu, and Q_{Load} = 0.45 pu, and the solar irradiation of the first DG is kept constant; while the solar irradiation of DG_2 drops in steps. It is noted that to simplify the comparison, all results are presented in pu based on the total system rating (not each PV system). It is noted that since most practical loads are RL loads, the simulation scenarios only consider cases where the converters inject reactive power. However, the proposed method is also applicable for RC loads.

5.1.1. Scenario 1: Static P and Static Q

The network in Fig. 4 was simulated while $R_{v\alpha}$ and $R_{v\beta}$ are set according to the fixed rated capacity using (10). As shown in Fig. 10, up to *t* = 5s, since the available solar power (P_{avail1} and P_{avail2} in Fig. 10.a) on both systems are equal (i.e., $1pu_{pv}$), the P_{Load} is shared in proportion to the rated capacity of each DGs. However, as soon as the solar irradiation of DG_2 drops (Fig. 10.a), a new operating voltage is imposed on the entire MG that forces the DG_1 (as well as the DG_2) to reduce its generation (Fig. 10.b) despite the fact that its solar irradiation is not changed (Fig. 10.a). Consequently, the total generation $< P_{Load}$, which in turn reduces V_{DC} to compensate for the energy shortage. When $V_{DC} < 0.85$ pu, the AG is turned on to supply the shortage. It is important to note that over the entire simulation $(P_{avail1} + P_{avail2}) > P_{Load}$, which demonstrates the inefficient use of the AG.

The available reactive power is shown in Fig. 10.d, it is noted that Q_{avail1} and Q_{avail2} increase as P_1 and P_2 decrease, however, due to the fixed sharing ratio, the shared reactive power (based on the fixed sharing ratio) from DG_1 and DG_2 remain constant for the entire simulation time (Fig. 10.e).

5.1.2. Scenario 2: Adaptive P and Static Q

The simulation of the virtual resistance scheme in Fig. 4 was repeated with $R_{v\alpha}$ varies according to (15) while $R_{v\beta}$ (i.e., *Q* sharing) remain constant according to (10). The results in Fig. 11.b illustrates that the power is proportionally shared according to the rated capacity of each DG when the solar irradiance is the same (i.e. up to *t*

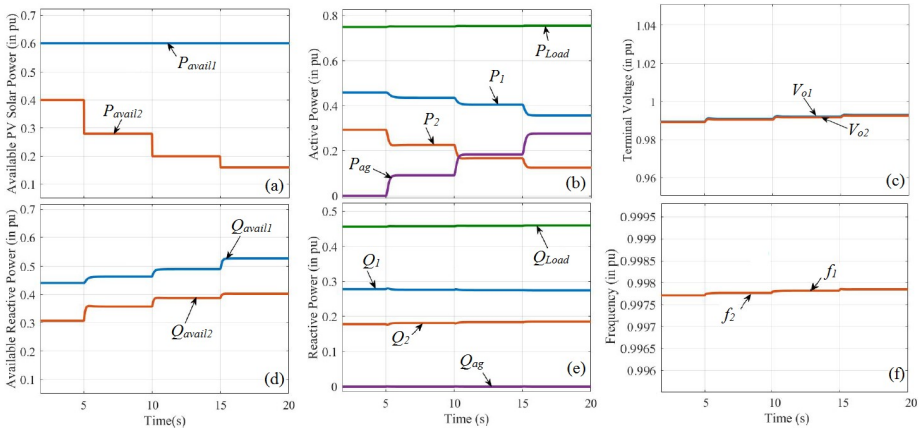

Figure 10: Virtual resistance load sharing simulation of two DG systems using **Static *P*** and **Static *Q*** scheme

= 5s). As soon as the P_{avail2} (Fig. 11.a) reduces, the $R_{v\alpha}$ of DG_2 increases which reduces P_2 (Fig. 11.b). However, due to the use of the adaptive $R_{v\alpha}$, the $R_{v\alpha}$ of DG_1 proportionally reduces, which increases P_1 (Fig. 11.b). In other words, DG_1 compensates for DG_2 (since DG_1 has extra capacity), which leads to $P_{ag} = 0$, as shown in Fig. 11.b.

Fig. 11.e shows the reactive power interaction for Q_{Load} sharing: the reactive power (based on fixed $R_{v\beta}$) from DG_1 and DG_2 remain constant until t = 15s, which demonstrates the effectiveness of the virtual resistance scheme in decoupling and independently sharing P_{Load} and Q_{Load} based on $R_{v\alpha}$ and $R_{v\beta}$ respectively. Figure 11.d shows Q_{avail} for DG_1 and DG_2. It is noted that Q_{avail1} drops as P_1 increases while Q_{avail2} increases as P_2 drops. However, due to fixed $R_{v\beta}$ (as shown in Fig. 11.e), Q_1 and Q_2 remain constant (until t = 15s) regardless of their Q_{avail}. At t = 15s, $Q_{DG1} > Q_{avail1}$; hence according to Fig. 9, AG is triggered ON to compensate for the deficiency in the reactive power supply (Fig. 11.e). It is noted that although Q_{avail2} increase, Q_2 remain constant which demonstrates an inefficient Q sharing.

5.1.3. Scenario 3: Adaptive P and Adaptive Q

The simulation was repeated while $R_{v\alpha}$ and $R_{v\beta}$ vary according to (15), using the proposed method illustrated in Fig. 8a. Fig. 12.b shows that P is dynamically shared appropriately based on available generation. In addition, as shown in Fig.

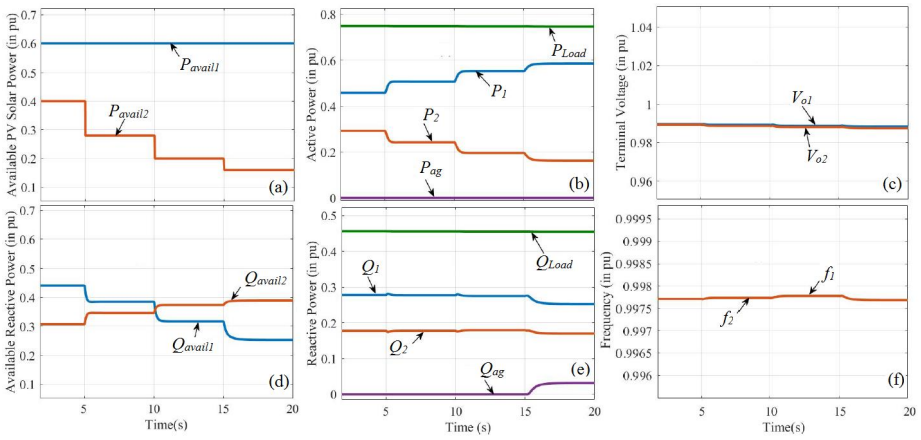

Figure 11: Virtual resistance load sharing simulation of two DG systems using **Adaptive *P*** and **Static *Q*** scheme

12.e, reactive powers are now adaptively regulated, so that contributed reactive power changes proportional to Q_{avail1} variations: increase in P_1 to compensate drop in P_2 will result in a reduction in Q_{avail1}; hence the adaptive $R_{v\beta}$ conditions a decrease in Q_1 and an equivalent increase in Q_2 (since Q_{avail2} increases as P_2 drops). As a result, the switching stress on each DG's converter is reduced since unit with more P generation has less contribution to Q_{Load}.

Moreover, Fig. 12.e now shows zero reactive power demand from the AG, unlike Fig. 11.e, which indicates that units compensate for each other. As it can be seen from Fig. 13, where the THD of the output voltage of the three test scenarios are compared, the THD of case iii (i.e., adaptive P and adaptive Q) is much less than the other schemes.

5.2. Virtual Resistance Load Sharing using Real-Time Solar Irradiance Variation

The real solar irradiation profiles (shown in Fig. 14.a), which are measured at the College of Engineering, are also used to compare the static virtual resistance sharing with the proposed adaptive one. P_{Load} and Q_{Load} are kept constant at 0.75 pu and 0.45 pu, respectively. Fig. 14.b indicates that the adaptive virtual resistance load sharing scheme offers more energy saving (up to 89% for the given solar irradiation) from the AG when compared with the static virtual resistance load sharing scheme.

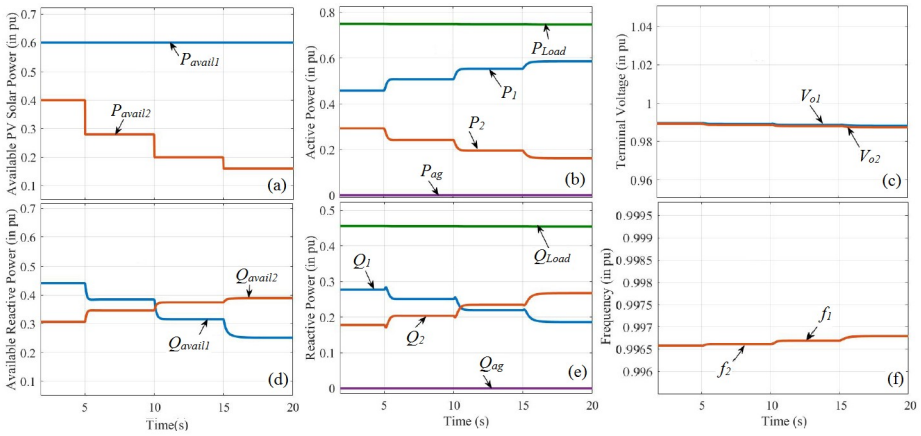

Figure 12: Virtual resistance load sharing simulation of two DG systems using using **Adaptive *P*** and **Adaptive *Q*** scheme

A quantity, similar to energy, is also required to compare the reactive power from the AG for the static and adaptive virtual resistance load sharing schemes. The term "reactive energy" is thus introduced; which is the integral of the AG's reactive power. As shown in Fig. 14.c, the adaptive virtual resistance sharing scheme requires much less "reactive energy" from the AG in comparison with that of the static virtual resistance.

6. Conclusion

This paper proposes a virtual impedance control scheme in which the virtual reactance is used to decouple the active and reactive power control (in a resistive microgrid); while the virtual resistance (in $\alpha\beta$ frame) is used to independently control the active and reactive power. This paper also proposes a method to dynamically vary the virtual resistance value (in $\alpha\beta$ frame) such that the load sharing (for both active and reactive powers) becomes sensitive to the intermittent nature of the input solar power. The simulation results demonstrate that using the proposed scheme, as long as the solar irradiation levels are the same on DG units, similar to conventional static sharing, the load is shared in proportion to the units' ratings. However, in cases of unequal irradiance, the units can compensate for each other (if sufficient capacity is

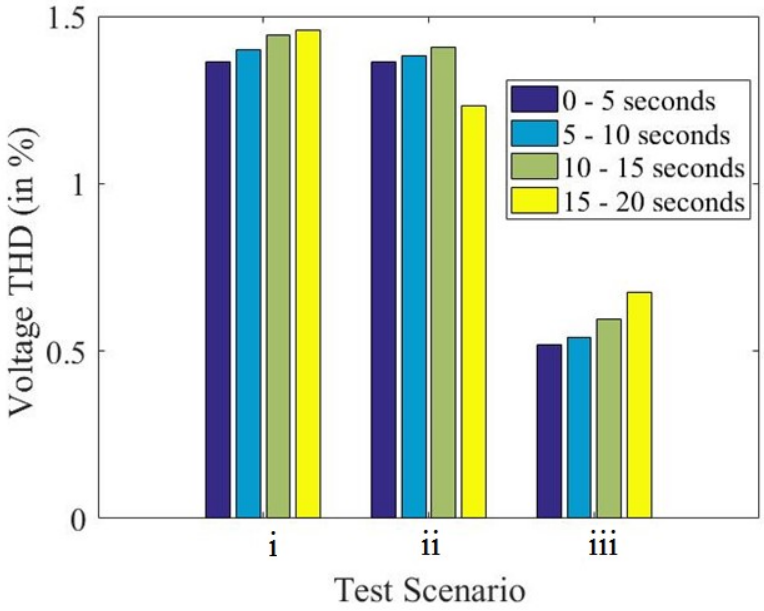

Figure 13: Bar charts illustrating the output voltage's Total Harmonic Distortion (THD) for the three test scenarios: (i) Static P and Static Q; (ii) Adaptive P and Static Q; (iii) Adaptive P and Adaptive Q

available), which provides significant energy saving. It is also shown that using the proposed method the switching stresses on the inverters are reduced by dynamically regulating the reactive power sharing, through reducing the reactive power contribution of units with higher active power contribution. It was shown that the adaptive reactive power contribution also reduces the demanded reactive power from a local auxiliary generator as well as the total harmonic distortion content.

References

[1] H. Mahmood, D. Michaelson, J. Jiang, A power management strategy for pv/battery hybrid systems in islanded microgrids, IEEE Emerging and Selected Topics in Power Electron 2 (4) (2014) 870–882. doi:10.1109/JESTPE.2014.2334051.

[2] K. T. Tan, X. Y. Peng, P. L. So, Y. C. Chu, M. Z. Q. Chen, Centralized control for parallel operation of distributed generation inverters in microgrids, IEEE Trans-

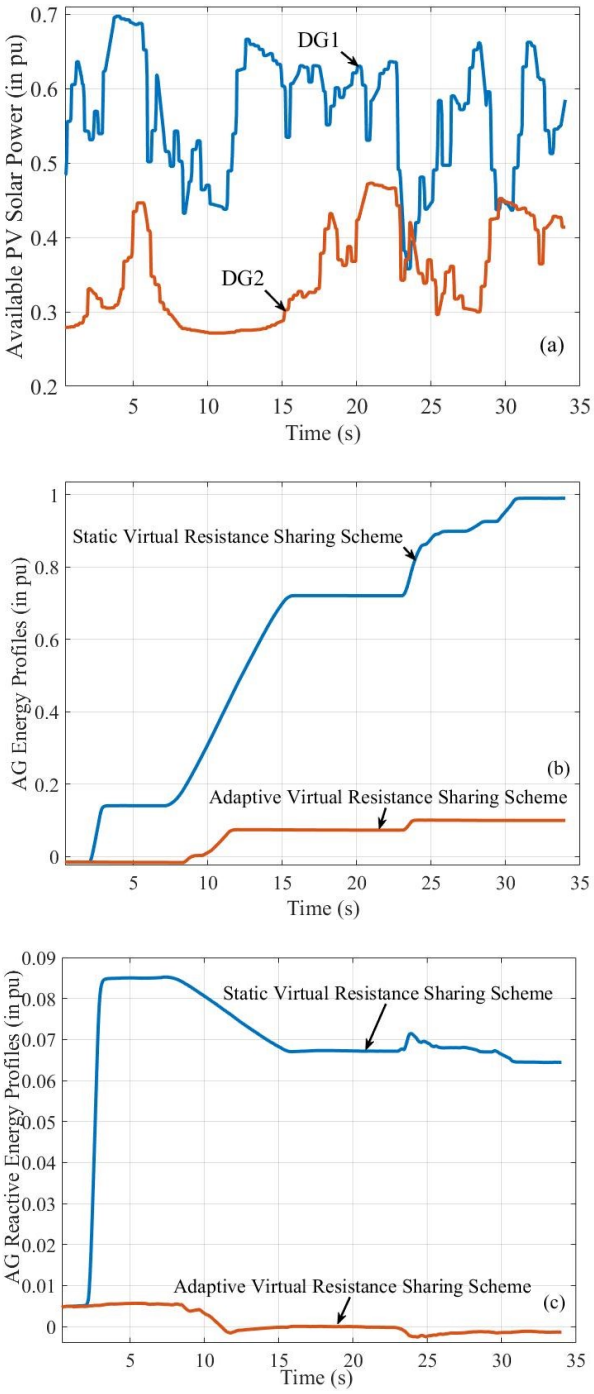

Figure 14: Static and adaptive virtual resistance sharing schemes simulation of two DG systems using the real-time solar data

actions on Smart Grid 3 (4) (2012) 1977–1987. doi:10.1109/TSG.2012.2205952.

[3] J. Y. Kim, J. H. Jeon, S. K. Kim, C. Cho, J. H. Park, H. M. Kim, K. Y. Nam, Cooperative control strategy of energy storage system and microsources for stabilizing the microgrid during islanded operation, IEEE Transactions on Power Electronics 25 (12) (2010) 3037–3048. doi:10.1109/TPEL.2010.2073488.

[4] M. Mehrasa, E. Pouresmaeil, H. Mehrjerdi, B. N. Jrgensen, J. Catalo, Control technique for enhancing the stable operation of distributed generation units within a microgrid, Energy Conversion and Management 97 (Supplement C) (2015) 362 – 373. doi:https://doi.org/10.1016/j.enconman.2015.03.078.

[5] Y. W. Li, C. N. Kao, An accurate power control strategy for power-electronics-interfaced distributed generation units operating in a low-voltage multibus microgrid, IEEE Transactions on Power Electronics 24 (12) (2009) 2977–2988. doi:10.1109/TPEL.2009.2022828.

[6] M. Fazeli, G. M. Asher, C. Klumpner, L. Yao, Novel integration of dfig-based wind generators within microgrids, IEEE Transactions on Energy Conversion 26 (3) (2011) 840–850. doi:10.1109/TEC.2011.2146253.

[7] V. Mortezapour, H. Lesani, Hybrid ac/dc microgrids: A generalized approach for autonomous droop-based primary control in islanded operations, International Journal of Electrical Power and Energy Systems 93 (Supplement C) (2017) 109 – 118. doi:https://doi.org/10.1016/j.ijepes.2017.05.022.
URL http://www.sciencedirect.com/science/article/pii/S0142061517306087

[8] M. Fazeli, J. B. Ekanayake, P. M. Holland, P. Igic, Exploiting pv inverters to support local voltage:a small-signal model, IEEE Transactions on Energy Conversion 29 (2) (2014) 453–462. doi:10.1109/TEC.2014.2300012.

[9] J. M. Guerrero, L. Hang, J. Uceda, Control of distributed uninterruptible power supply systems, IEEE Transactions on Industrial Electronics 55 (8) (2008) 2845–2859. doi:10.1109/TIE.2008.924173.

[10] M. Nandurkar, M. Rajeev, Design and simulation of three phase inverter for grid connected photovoltaic systems, Proceeding Of Third Biennial National Conference, NCNTE (2012) 80–83.

[11] Y. A. R. I. Mohamed, E. F. El-Saadany, Adaptive decentralized droop controller to preserve power sharing stability of paralleled inverters in distributed generation microgrids, IEEE Transactions on Power Electronics 23 (6) (2008) 2806–2816. doi:10.1109/TPEL.2008.2005100.

[12] R. G. Wandhare, S. Thale, V. Agarwal, Design of a photovoltaic power conditioning system for hierarchical control of a microgrid, in: 2014 IEEE 40th Photovoltaic Specialist Conference (PVSC), 2014, pp. 3144–3149. doi:10.1109/PVSC.2014.6925603.

[13] J. M. Guerrero, J. Matas, L. G. de Vicuna, M. Castilla, J. Miret, Decentralized control for parallel operation of distributed generation inverters using resistive output impedance, IEEE Transactions on Industrial Electronics 54 (2) (2007) 994–1004. doi:10.1109/TIE.2007.892621.

[14] J. Rocabert, G. M. S. Azevedo, A. Luna, J. M. Guerrero, J. I. Candela, P. Rodrguez, Intelligent connection agent for three-phase grid-connected microgrids, IEEE Transactions on Power Electronics 26 (10) (2011) 2993–3005. doi:10.1109/TPEL.2011.2116126.

[15] R. Majumder, B. Chaudhuri, A. Ghosh, R. Majumder, G. Ledwich, F. Zare, Improvement of stability and load sharing in an autonomous microgrid using supplementary droop control loop, IEEE Transactions on Power Systems 25 (2) (2010) 796–808. doi:10.1109/TPWRS.2009.2032049.

[16] P. Sreekumar, V. Khadkikar, A new virtual harmonic impedance scheme for har-

monic power sharing in an islanded microgrid, IEEE Transactions on Power Delivery 31 (3) (2016) 936–945. doi:10.1109/TPWRD.2015.2402434.

[17] Y. Guan, J. C. Vasquez, J. M. Guerrero, E. A. A. Coelho, Small-signal modeling, analysis and testing of parallel three-phase-inverters with a novel autonomous current sharing controller, in: 2015 IEEE Applied Power Electronics Conference and Exposition (APEC), 2015, pp. 571–578. doi:10.1109/APEC.2015.7104406.

[18] Y. Guan, J. C. Vasquez, J. M. Guerrero, A simple autonomous current-sharing control strategy for fast dynamic response of parallel inverters in islanded microgrids, in: 2014 IEEE International Energy Conference (ENERGYCON), 2014, pp. 182–188. doi:10.1109/ENERGYCON.2014.6850426.

[19] J. Kim, J. M. Guerrero, P. Rodriguez, R. Teodorescu, K. Nam, Mode adaptive droop control with virtual output impedances for an inverter-based flexible ac microgrid, IEEE Transactions on Power Electronics 26 (3) (2011) 689–701. doi:10.1109/TPEL.2010.2091685.

[20] R. Majumder, A. Ghosh, G. Ledwich, F. Zare, Load sharing and power quality enhanced operation of a distributed microgrid, IET Renewable Power Generation 3 (2) (2009) 109–119. doi:10.1049/iet-rpg:20080001.

[21] Q. C. Zhong, Y. Zeng, Universal droop control of inverters with different types of output impedance, IEEE Access 4 (2016) 702–712. doi:10.1109/ACCESS.2016.2526616.

[22] J. He, Y. W. Li, J. M. Guerrero, F. Blaabjerg, J. C. Vasquez, An islanding microgrid power sharing approach using enhanced virtual impedance control scheme, IEEE Transactions on Power Electronics 28 (11) (2013) 5272–5282. doi:10.1109/TPEL.2013.2243757.

[23] Y. Zhu, F. Zhuo, B. Liu, H. Yi, An enhanced load power sharing strategy for low-voltage microgrids based on inverse-droop control method, in: 2014 Inter-

national Power Electronics Conference (IPEC-Hiroshima 2014 - ECCE ASIA), 2014, pp. 3546–3552. doi:10.1109/IPEC.2014.6870006.

[24] J. He, Y. W. Li, An enhanced microgrid load demand sharing strategy, IEEE Transactions on Power Electronics 27 (9) (2012) 3984–3995. doi:10.1109/TPEL.2012.2190099.

[25] J. He, Y. W. Li, Generalized closed-loop control schemes with embedded virtual impedances for voltage source converters with lc or lcl filters, IEEE Transactions on Power Electronics 27 (4) (2012) 1850–1861. doi:10.1109/TPEL.2011.2168427.

[26] X. Tang, X. Hu, N. Li, W. Deng, G. Zhang, A novel frequency and voltage control method for islanded microgrid based on multienergy storages, IEEE Transactions on Smart Grid 7 (1) (2016) 410–419. doi:10.1109/TSG.2014.2381235.

[27] A. H. Etemadi, E. J. Davison, R. Iravani, A generalized decentralized robust control of islanded microgrids, IEEE Transactions on Power Systems 29 (6) (2014) 3102–3113. doi:10.1109/TPWRS.2014.2312615.

[28] D. Wu, F. Tang, J. M. Guerrero, J. C. Vasquez, G. Chen, L. Sun, Autonomous active and reactive power distribution strategy in islanded microgrids, in: 2014 IEEE Applied Power Electronics Conference and Exposition - APEC 2014, 2014, pp. 2126–2131. doi:10.1109/APEC.2014.6803600.

[29] H. Gu, X. Guo, W. Wu, Accurate power sharing control for inverter-dominated autonomous microgrid, in: Proceedings of The 7th International Power Electronics and Motion Control Conference, Vol. 1, 2012, pp. 368–372. doi:10.1109/IPEMC.2012.6258879.

[30] Y. Zhu, F. Zhuo, H. Shi, Accurate power sharing strategy for complex microgrid based on droop control method, in: 2013 IEEE ECCE Asia Downunder, 2013, pp. 344–350. doi:10.1109/ECCE-Asia.2013.6579119.

[31] K. D. Brabandere, B. Bolsens, J. V. den Keybus, A. Woyte, J. Driesen, R. Belmans, A voltage and frequency droop control method for parallel inverters, IEEE Trans-

actions on Power Electronics 22 (4) (2007) 1107–1115. doi:10.1109/TPEL.2007.900456.

[32] A. M. Egwebe, M. Fazeli, P. Igic, P. M. Holland, Implementation and stability study of dynamic droop in islanded microgrids, IEEE Transactions on Energy Conversion 31 (3) (2016) 821–832. doi:10.1109/TEC.2016.2540922.

[33] A. Yazdani, P. P. Dash, A control methodology and characterization of dynamics for a photovoltaic (pv) system interfaced with a distribution network, IEEE Transactions on Power Delivery 24 (3) (2009) 1538–1551. doi:10.1109/TPWRD.2009.2016632.

[34] D. Mohan, T. M. Udeland, W. P. Robbins, Power Electronics Converters, Applications, and Design, 3rd Edition, John Wiley and Sons, 2003.

[35] M. Fazeli, P. Igic, P. Holland, R. P. Lewis, Z. Zhou, Novel maximum power point tracking with classical cascaded voltage and current loops for photovoltaic systems, in: IET Conference on Renewable Power Generation (RPG 2011), 2011, pp. 1–5. doi:10.1049/cp.2011.0109.

[36] K. Kelesidis, G. Adamidis, G. Tsengenes, Investigation of a control scheme based on modified p-q theory for single phase single stage grid connected pv system, in: 2011 International Conference on Clean Electrical Power (ICCEP), 2011, pp. 535–540. doi:10.1109/ICCEP.2011.6036286.

[37] V. F. Pires, J. Martins, C. Hao, Dual-inverter for grid-connected photovoltaic system: Modeling and sliding mode control, Solar Energy 86 (7) (2012) 2106 – 2115. doi:https://doi.org/10.1016/j.solener.2012.04.012.